WARSAW UNIVERSITY OF TECHNOLOGY Index 351733
FACULTY OF CIVIL ENGINEERING
COMMITTEE FOR CIVIL AND WATER ENGINEERING
POLISH ACADEMY OF SCIENCES ISSN 1230-2945

DOI: 10.24425/ace.2025.153330
ARCHIVES OF CIVIL ENGINEERING
Vol. LXXI ISSUE 1 2025
pp. 203–223

Research paper

Rheological performance of Portland cement pastes containing different fineness of circulating fluidized bed combustion ashes

Lei Zhang[1]

Abstract: Circulating fluidized bed combustion (CFBC) ash, a by-product of fluidized bed coal-fired sulfur fixation technology, presents an opportunity for recycling and reuse when employed as a supplementary cementitious material in cement composite systems, thereby alleviating environmental pressure. Meanwhile, the rheological characteristics of cement pastes are crucial for optimizing its workability, facilitating diverse engineering applications such as pumping, formwork pressure calculation, and 3D printing. Against this backdrop, this study systematically explores the impact of CFBC ash, varying in particle size and content, on the rheological properties of Portland cement (PC) paste. Findings reveal that elevated CFBC content correlates with heightened yield stress and viscosity of the paste, with the paste incorporating 40% CFBC ash having the highest yield stress of 71.6 Pa. Furthermore, incorporating CFBC with finer particle size distribution amplifies these rheological parameters. Thixotropy mirrors the alterations in dynamic yield stress and viscosity, indicating that CFBC ash addition enhances paste thixotropy. In PC-CFBC ash composites, G' values consistently surpass G'', suggesting early-stage elasticity during oscillation testing. Thixotropy in PC-CFBC ash composites is intricately linked to superplasticizer adsorption capacity, while viscoelastic evolution of the paste is governed by hydration kinetics.

Keywords: circulating fluidized combustion ashes, Portland cement, rheology, hydration, adsorption amount

[1]MSc. Eng., Changzhi Vocational and Technical College, Changzhi 046000, China, e-mail: 36696949@qq.com, ORCID: 0009-0008-2869-037X

1. Introduction

Amidst the rapid advancement of science and technology, the significance of non-renewable resources has surged, accentuating the imperative for reutilizing diverse industrial waste and fostering novel resource development to underpin sustainable progress in the 21st century [1–4]. Coal, Earth's most abundant and widely distributed fossil fuel, historically engenders substantial emissions of sulfur dioxide and nitrogen oxides through traditional combustion processes [5,6]. Circulating fluidized bed combustion (CFBC) technology, an innovative boiler paradigm supplanting conventional pulverized coal combustion (PCC) boilers, has garnered widespread adoption due to its economical investment outlay, robust desulfurization efficacy, diminished combustion temperatures, and reduced nitrogen oxide discharges [7–11]. In CFBC boilers, sulfur dioxide mitigation is facilitated by introducing limestone or dolomite during combustion, with optimal SO_2 capture efficiency typically achieved at a Ca/S ratio of 2.0 to 2.5 [12–15]. Notably, CFBC operation entails lower combustion temperatures (850–900°C) compared to PCC methods [14, 16]. Taking limestone addition as a case in point, the sulfur fixation process unfolds in two distinct stages [17]:

$$CaCO_3 \rightarrow CaO + CO_2 \tag{1.1}$$

$$CaO + SO_2 + 1/2O_2 \rightarrow CaSO_4 \tag{1.2}$$

CFBC ash denotes the solid residue discharged subsequent to the combustion of sulfur-containing coal and a sulfur-fixing agent in a predetermined ratio within a fluidized bed to effect sulfur capture [17]. This residue encompasses both flue-collected CFBC ash and bottom furnace-discharged CFBC slag. The release of CFBC ash constitutes a significant portion of total ash emissions, predominantly comprising free lime (f-CaO) and sulfur trioxide (SO_3) [18]. Owing to the limited utilization of calcium adsorbents, the residual calcium oxide content in CFBC ash typically ranges between 20% to 30% [19]. Notably, the characteristics of discharged CFBC ash markedly diverge from those of waste (fly ash) generated during coal powder combustion at approximately 1300°C due to the lower combustion temperatures in circulating fluidized bed boilers, precluding the formation of a liquid phase [20]. CFBC ash tends to exhibit a loose and porous structure, necessitating substantially higher water demand compared to fly ash. Furthermore, the presence of f-CaO and $CASO_4$ confers notable pozzolanic and hydraulic properties, self-cementing, and expansiveness upon CFBC ash [19,21,22]. Variations in coal composition, sulfur fixation agents, combustion efficiency, and sulfur fixation effectiveness yield disparities in the quality of CFBC ash. The accumulation of such ash not only engenders considerable land occupancy but also poses environmental hazards. Thus, to foster global-scale adoption of CFBC technology, the imperative challenge lies in the comprehensive utilization of CFBC ash.

Currently, CFBC ash finds extensive application in the realm of construction materials, including in the synthesis of geopolymers [24], non-autoclaved aerated concretes [25], and production of autoclaved bricks [26]. Numerous scholarly investigations have explored the utilization of CFBC ash as a supplementary cementitious material in cement-based composites [10, 19, 20, 27]. Substituting ordinary Portland cement (PC) and low-alkali cement

with CFBC ash has been noted to mitigate shrinkage-induced cracking in hardened pastes, thereby enhancing the volume stability post-hardening [20, 27]. A novel cementitious material, referred to as cement-free cementitious material (GFA) cement, is attainable by blending mineral admixtures such as CFBC ash, fly ash, and ground granulated blast furnace slag (GGBFS) [10, 19, 28]. The hydration products of GFA cement primarily encompass ettringite, hydrated calcium silicates and aluminosilicates, sulfoaluminates, and calcium hydroxide. The augmentation of CFBC fly ash content accelerates early hydration rates, yielding a denser microstructure and bolstering resistance to sulfate attack [29–31]. Concomitantly, the inclusion of CFBC ash yields diverse types of hydration products of alkali-activated slag (AAS), culminating in increased pore volume [32]. Incorporating a modest proportion of CFBC ash enhances the compressive strength, bond performance, and durability of hardened self-compacting concrete (SCC) [33]. Moreover, the 28-day compressive strength of high-performance concrete (HPC) blended with 20% CFBC ash surpasses that of concrete with equivalent fly ash content, while exhibiting lesser quality and strength degradation post-freeze-thaw cycles [34]. Augmenting with activators such as sodium carbonate and sodium hydroxide can expedite the strength development rate of hardened pastes [35–37].

The rheological characteristics serve as pivotal indicators of the flow properties of fresh cementitious materials [38, 39]. They hold particular significance in predicting the pumpability, multi-layer casting, and compactibility, which are crucial attributes in materials utilized for 3D printing [40, 41]. The rheological behavior of cement paste is typically assessed and quantified employing specific rheological models, with the Bingham model standing out as the most renowned and widely utilized among them [42, 43]. However, given that most cement-based materials exhibit non-Newtonian fluid attributes, characterized by non-linear variations in shear stress with shear rate and the presence of yield stress, alternative models such as the Herschel–Bulkley model, modified Bingham model, and Casson model have been introduced to capture the nonlinear rheological behavior. Furthermore, fresh cement paste represents a reactive suspension system. As cement continuously hydrates and generates hydration products, the flowability of the paste gradually diminishes due to alterations in its internal microstructure, transitioning from initially predominant plastic behavior to predominantly elastic behavior [44–46]. Consequently, in addition to employing rheological models for characterizing rheological parameters, the viscoelasticity and thixotropy of the paste stand out as vital properties for delineating the evolving microstructural changes over time [47–50].

Considering the scarcity of research on the rheological characteristics of PC paste subsequent to the incorporation of CFBC ash, this study seeks to elucidate the early rheological attributes of composite paste via dynamic rheological measurements, thixotropy assessment, and viscoelasticity analysis. Subsequently, adsorption capacity of polycarboxylate superplasticizer (PCE) and hydration heat release rate were employed to quantify the degree of dispersion of flocculated structures, and rate of hydration product generation in the fresh cement composite, respectively. Ultimately, by scrutinizing the dispersion state of suspended particles, the efficacy of PCE in adsorption and dispersion, and the kinetics of hydration, this study delves into the mechanistic influence of CFBC ash on the rheological characteristics of cement paste.

2. Materials and methodology

2.1. Materials and sample preparation

Ordinary Portland cement (OPC) Type I 42.5 produced by China United Cement Corporation (conforming to the Chinese Standard GB175-2007), CFBC ash and polycarboxylate superplasticizer (PCE) provided by Hubei Yihua Group Co., Ltd. with 27% water reducing rate were used in this study. On the basis of the original CFBC ash, two types of CFBC ash with finer particle size were obtained by using a ball mill to grind the CFBC ash to varying degrees. The three types of CFBC ashes were recorded as CFBC1, CFBC2, and CFBC3 in descending order of specific surface area. The chemical properties of OPC and CFBC ashes were summarized in Table 1, and the particle size distribution and SEM images (FEI Quanta 200 FEG ESEM) of three CFBC ashes were presented in Fig. 1 and Fig. 2, respectively.

Table 1. Chemical and physical properties of OPC and CFBC ash

	Chemical composition (%)								Physical properties	
	CaO	SiO_2	Al_2O_3	Fe_2O_3	MgO	SO_3	Na_2O	Loss on ignition (%)	Density (g/cm^3)	Specific surface area (m^2/kg)
OPC	63.5	20.6	4.6	3.1	3.4	2.21	0.53	2.12	3.14	344
CFBC ash	46.51	36.93	5.08	0.37	2.42	0.61	0.19	0.48	2.89	316

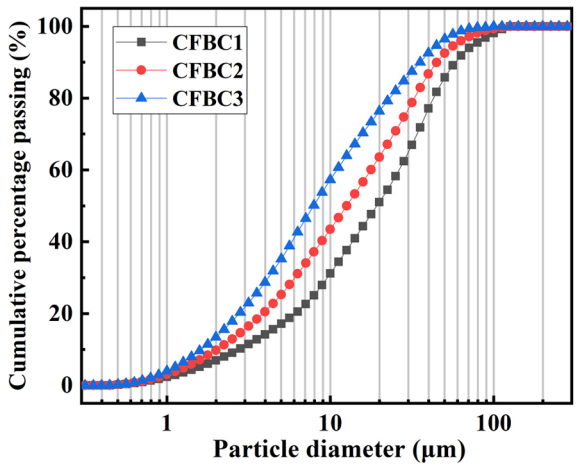

Fig. 1. Particle size distribution of three CFBC ashes

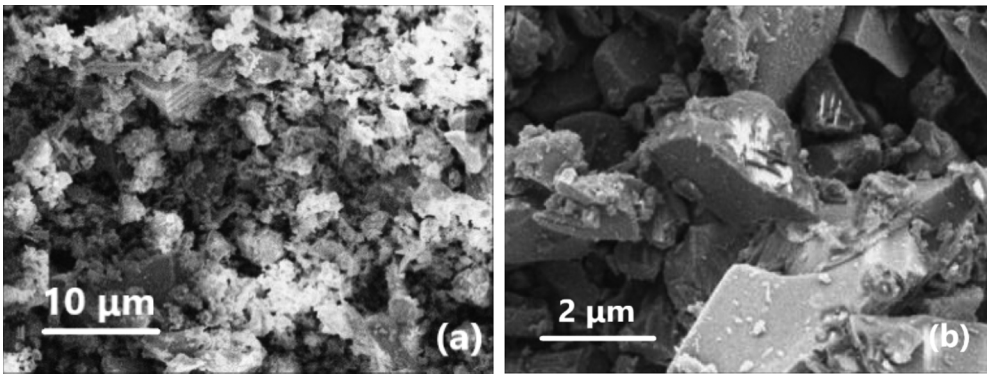

Fig. 2. SEM images of CFBCA1 at different scales showing: (a) 10 µm, (b) 2 µm

The mix proportions used in this study are shown in Table 2. A certain amount of OPC, CFBC ash, water, and PCE according to the corresponding mix proportion were first weighed, then the powder materials were put into a mixing pot and stirred evenly. Water and PCE were added into the powder. The stirring system was to first stir at 60 rpm for 90 seconds, then stop for 15 seconds before stirring at 120 rpm for 90 seconds.

Table 2. Mix proportion of PC pastes incorporating CFBC ashes and PCE

No.	Sample	Binder compositions (wt.%)				Water (wt.%)	PCE (wt.%)
		PC	CFBC1	CFBC2	CFBC3		
1	PC	100	0	0	0	35	0.1
2	10CFBC1	90	10	0	0	35	0.1
3	20CFBC1	80	20	0	0	35	0.1
4	30CFBC1	70	30	0	0	35	0.1
5	40CFBC1	60	40	0	0	35	0.1
6	10CFBC2	90	0	10	0	35	0.1
7	20CFBC2	80	0	20	0	35	0.1
8	30CFBC2	70	0	30	0	35	0.1
9	40CFBC2	60	0	40	0	35	0.1
10	10CFBC3	90	0	0	10	35	0.1
11	20CFBC3	80	0	0	20	35	0.1
12	30CFBC3	70	0	0	30	35	0.1
13	40CFBC3	60	0	0	40	35	0.1

2.2. Testing procedures

2.2.1. Rheological tests

The experiment was conducted under ambient temperature of (20 ± 1)°C and relative humidity of (70 ± 3)%. An Anton Paar MCR 102 rheometer was used to test the rheological parameters of the paste. An appropriate amount of evenly stirred paste was taken and poured into the rheometer cup. The rotor height was set to a constant value, where the inner diameter of the rotor system was 11 mm and the outer diameter was 21 mm. The outer cylinder was kept stationary through a fixture during the testing process.

In this study, dynamic rheological testing was divided into three stages: Ascending, constant, and descending. Firstly, a pre shear rate of 100 s^{-1} was applied to the paste to ensure that each group maintains the same uniform state before testing. The shear rate of the ascending section increases linearly from 0 s^{-1} to 100 s^{-1}, followed by a constant shear rate of 30 s, and finally decreases from 100 s^{-1} to 0 s^{-1} [48]. Fig. 3 shows a typical rheological curve using a three-stage testing system. It can be observed from Fig. 3 that although there was pre shear, there were still many fluctuation points in the shear rate in the ascending section. In order to reduce the error of these unstable data points in rheological testing, the shear stress-shear rate relationship in the descending section was used to fit the rheological parameters, and the 20–80 s^{-1} section was used to calculate the area of the thixotropic hysteresis loop. However, sometimes using only a thixotropic loop to evaluate the thixotropy may cause certain errors [51]. Considering this, the three interval thixotropy test (3ITT) [47, 52] and thixotropy index [53] can also be used to evaluate the reversible structural changes of cement pastes under external shear forces. Fig. 4 shows the viscosity variation of cement paste based on the 3ITT method. The structural

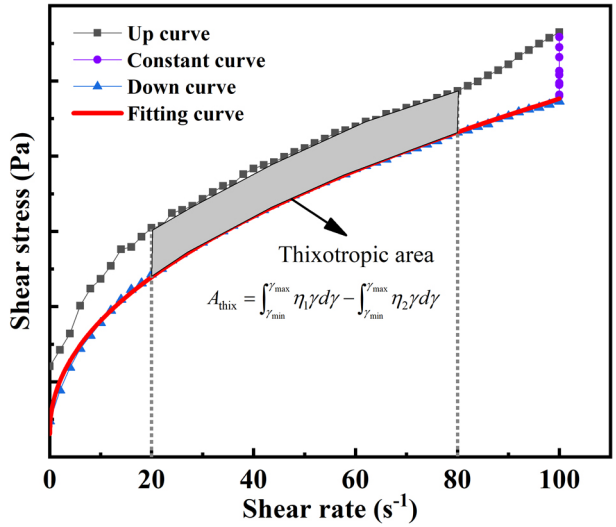

Fig. 3. Three stage rheological curves for dynamic rheological testing and calculation of rheological parameters and thixotropic loop area

recovery rate of cement paste can be expressed by Eq. (2.1), where η_1 and η_0 represents the recovery apparent viscosity and initial apparent viscosity of the paste, respectively.

$$R = \frac{\eta_1}{\eta_0} \times 100\% \tag{2.1}$$

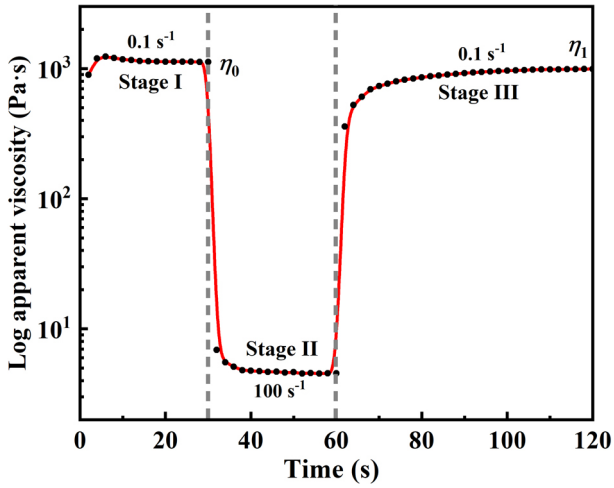

Fig. 4. A typical viscosity curve obtained using the 3ITT method

The viscoelasticity of cement paste was tested using dynamic shear rheometer (DSR) test. In this study, viscoelastic testing was divided into amplitude sweep and time sweep. In amplitude sweep, the frequency remains constant at 10 rad/s, and the amplitude increases logarithmically from 10^{-4}% to 10^{1}%. The storage modulus G' and loss modulus G'' of the paste are tested for their variation with amplitude. Time sweep controls the amplitude and frequency to remain constant at 10^{-4} and 1 Hz, respectively. G' and G'' were measured every 30 s for 120 min, and the phase angle was calculated by Eq. (2.2):

$$\tan\delta = \frac{G''}{G'} \tag{2.2}$$

2.2.2. Adsorption amount

The adsorption capacity of high molecular weight polymers such as PCE on the surface of cement particles can be characterized by the changes in carbon concentration of the solution before and after the addition of PCE. This study used the Total Organic Carbon (TOC) adsorption method to determine the adsorption performance of PCE. 50 g of paste was poured into a centrifuge tube and stirred with magnetic force for 3 min, and then centrifuged at a speed of 6000 r/min for 5 min. The upper clear liquid was collected and a 0.22 μ filter with a filter membrane was used. The 10 mL of clear liquid was diluted for 100 times, and finally TOC instrument was used to measure the organic matter content to calculate the adsorption amount.

2.2.3. Calorimetric test

The hydration heat flow and cumulative heat release of cement were tested using a TAM Air 8-channel isothermal calorimeter for a duration of 36 h. The time interval between two adjacent test points was 5 min.

In order to reveal the hydration mechanism of the PC-CFBC ash composites, based on the Krstulovic–Dabic kinetics model, the corresponding kinetic parameters can be obtained by combining the experimentally measured hydration heat release data with the kinetic equation [54,55]. The Krstulovic–Dabic model suggests that hydration reactions can be divided into three stages, and their respective kinetic equations are as follows:

Nucleation and crystal growth (NG):

$$[-\ln(1-\alpha)]^{1/n} = K_{\mathrm{NG}}(t-t_0) \tag{2.3}$$

Interactions at phase boundaries (I):

$$\left[1-(1-\alpha)^{1/3}\right]^{1} = K_I(t-t_0) \tag{2.4}$$

Diffusion (D):

$$\left[1-(1-\alpha)^{1/3}\right]^{2} = K_D(t-t_0) \tag{2.5}$$

Eqs. (2.5)–(2.7) can be differentiated to obtain the differential equation of hydration kinetics, as shown in Eqs. (2.6)–(2.8):

NG:

$$\frac{\mathrm{d}\alpha}{\mathrm{d}t} = F_1(\alpha) = K_{\mathrm{NG}} n(1-\alpha)[-\ln?(1-\alpha)]^{(n-1)/n} \tag{2.6}$$

I:

$$\frac{\mathrm{d}\alpha}{\mathrm{d}t} = F_2(\alpha) = 3K_I(1-\alpha)^{2/3} \tag{2.7}$$

D:

$$\frac{\mathrm{d}\alpha}{\mathrm{d}t} = F_3(\alpha) = \frac{3K_D(1-\alpha)^{2/3}}{2-2(1-\alpha)^{1/3}} \tag{2.8}$$

Where α is the degree of hydration, K_{NG}, K_I and K_D are the reaction rate constants for three stages, n is the reaction order, and t_0 is the end time of the induction period. Two hydration heat indicators of the composite paste can be measured by an isothermal calorimeter, namely the hydration heat flow $\mathrm{d}Q/\mathrm{d}t$ and cumulative heat release $Q(t)$. Before calculating the parameters of the hydration kinetics model, it is necessary to first determine the maximum heat release $Q_{\max}$ of each cement pastes by Eq. (2.9):

$$\frac{1}{Q(t)} = \frac{1}{Q_{\max}} + \frac{t_{50}}{Q_{\max}(t-t_0)} \tag{2.9}$$

where t_{50} is the time when the heat release reaches 50% of the maximum value $Q_{\max}$. According to Eq. (2.11), a linear equation for $1/Q(t) - 1/(t - t_0)$ can be drawn, and the $Q_{\max}$ of each mix proportion can be calculated through fitting. Then, based on Eq. (2.10) and Eq. (2.11), hydration heat data can be converted into the hydration degree α and hydration rate $d\alpha/\mathrm{d}t$ required for the Krstulovic–Dabic model:

$$\alpha(t) = \frac{Q(t)}{Q_{\max}} \tag{2.10}$$

$$\frac{\mathrm{d}\alpha}{\mathrm{d}t} = \frac{\mathrm{d}Q(t)}{\mathrm{d}t} \cdot \frac{1}{Q_{\max}} \tag{2.11}$$

In the process of calculating hydration kinetics parameters, it is necessary to first take the logarithm of both sides of the Eqs. (2.8)–(2.10). Using Eq. (2.8) as an example, the natural logarithm was taken at both ends of the equation and organized to obtain Eq. (2.12):

$$\ln(-\ln(1-\alpha)) = n \ln K_{\mathrm{NG}} + n \ln(t - t_0) \tag{2.12}$$

Substitute hydration degree α and time t into Eq. (2.12), and calculate $\ln(-\ln(1-\alpha))$ and $t - t_0$, then the dynamic parameters n and K_{NG} of the NG process can be obtained through linear fitting. Similarly, the hydration kinetic parameters for the other two stages can be obtained by Eq. (2.9) and Eq. (2.10). The relationship between $\mathrm{d}\alpha/\mathrm{d}t$ and α and three reaction equations, i.e., $F_1(\alpha)$, $F_2(\alpha)$, and $F_3(\alpha)$ can be shown in Fig. 5.

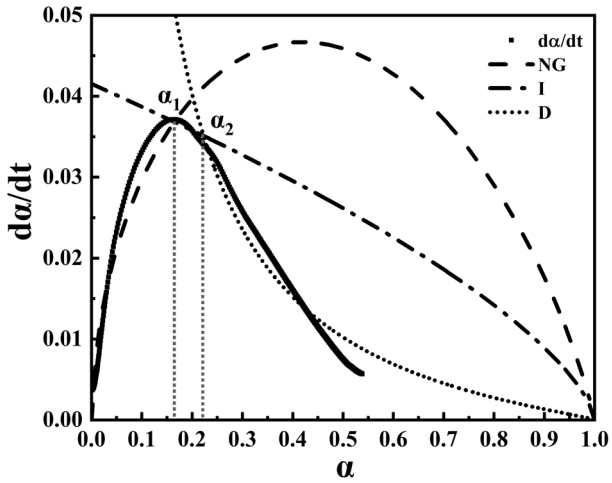

Fig. 5. Typical hydration reaction rate curve of paste calculated based on Krstulovic–Dabic model

3. Results

3.1. Dynamic rheology

Figure 6 shows the rheological curves of PC-CFBC ash blends under different CFBC ash contents and types. It can be observed that all pastes exhibit obvious shear thinning characteristics, that is, as the shear rate increases, the slope of shear stress-shear rate decreases continuously. In rheology, the tangent slope of a test point is considered as differential viscosity, and the ratio of shear stress to shear rate at that point is defined as apparent viscosity [42]. It can be observed that both differential viscosity and apparent viscosity decrease with increasing shear rate. The addition of CFBC ash significantly increases the shear stress of the paste at the same shear rate. In addition, under the same CFBC ash content, the paste containing CFBC3 exhibited the highest shear stress.

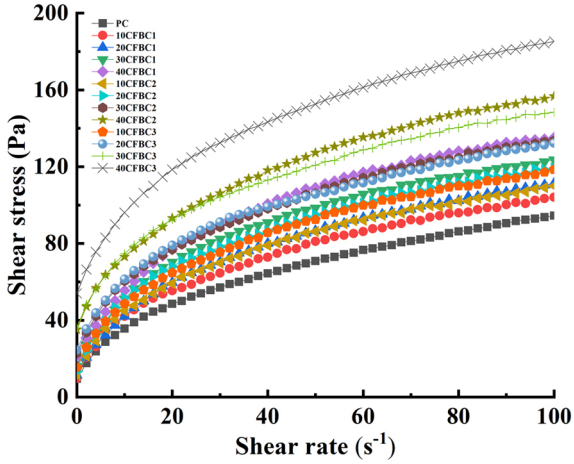

Fig. 6. Rheological curves of PC-CFBC ash blends under different mix ratios

Although Fig. 6 can display the rheological behavior of each group of pastes through rheological curves, it is not a quantitative comparison method. In order to more accurately compare the rheological properties of each sample horizontally, three rheological models were used to calculate the yield stress and viscosity, including modified Bingham model, Herschel–Bulkley model, and Casson model. Their expressions are shown in Eqs. (3.1)–(3.3) [56]:

$$\tau = \tau_0 + \mu \cdot \dot{\gamma} + c\dot{\gamma}^2 \tag{3.1}$$

$$\tau = \tau_0 + K\dot{\gamma}^n \tag{3.2}$$

$$\tau = \tau_0 + \eta_\infty \cdot \dot{\gamma} + 2(\tau_0\eta_\infty)^{1/2}\dot{\gamma}^{1/2} \tag{3.3}$$

where, τ_0 is the dynamic yield stress, μ is the apparent viscosity, c is the second-order parameter (Pa·s^2), K is the viscosity index, and n is the non-Newtonian index, η_∞ is the infinite viscosity. Fig. 7 shows the calculated results. It can be found that the calculation results based on different

rheological models have good consistency, and the R^2 of these three models can reach 0.95 or above, demonstrating good fitting accuracy. Consistent with the shear stress-shear rate relationship in Fig. 6, higher CFBC content corresponds to a higher yield stress and viscosity of the paste. In addition, the addition of CFBC with smaller particle size distribution further reduces the fluidity of the paste.

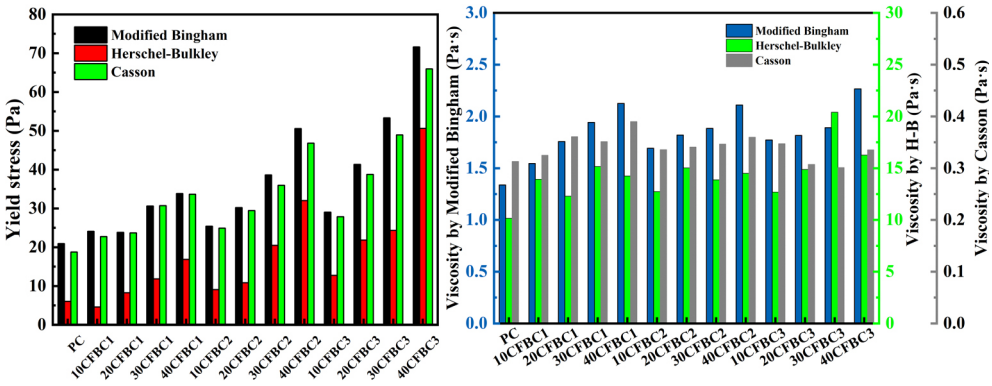

(a) (b)

Fig. 7. Rheological parameters of pastes based on different rheological models: (a) Yield stress, (b) viscosity

3.2. Thixotropy

Figure 8 shows the thixotropic parameters of each group of pastes. It can be observed that there is a smaller difference in the recovery rate obtained based on 3ITT among different mix proportions, while the thixotropic loop area shows a larger difference. The addition of

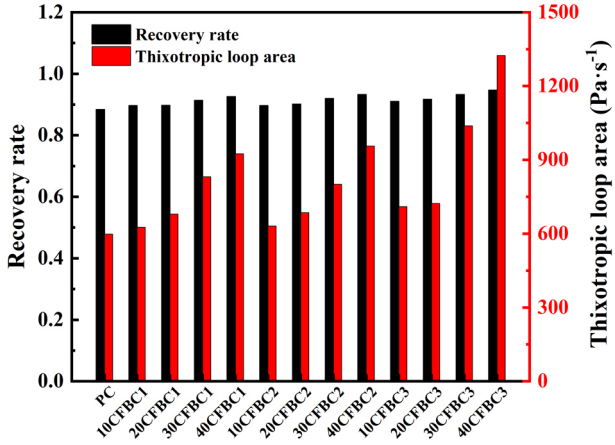

Fig. 8. Thixotropic parameters of PC-CFBCA mixes

CFBC ash significantly increases the thixotropy, similar to the trend of changes in rheological parameters. Taking the composite system containing CFBC1 as an example, when the content of CFBC1 increases from 0% to 40%, the recovery rate and thixotropic loop area increase from 0.8839 and 598 Pa·s^{-1} to 0.9258 and 924 Pa·s^{-1}, respectively. Among these 13 mix proportions, 40CFBC3 exhibited the highest thixotropy, with a thixotropic loop area of up to 1324 Pa·s^{-1}. This indicates that after undergoing high-speed shearing, the viscosity of the paste in this mix proportion decreases the most before and after shearing.

3.3. Viscoelasticity

3.3.1. Amplitude sweep

Figure 9 shows the evolution of the storage modulus G' and loss modulus G'' of the sample under different amplitude strains of oscillation. It can be observed from Fig. 9(a) that the two moduli of the paste containing CFBC ash will first remain constant, that is, the modulus does not change significantly with the increase of strain. This area is commonly referred to as the linear viscoelastic range (LVR), which is used to determine the critical strain. As the strain continues to increase, the two moduli begin to decrease and finally intersect at a certain point. This indicates that the internal structure of the paste has been destroyed and cannot exhibit significant elastic properties in a short period of time.

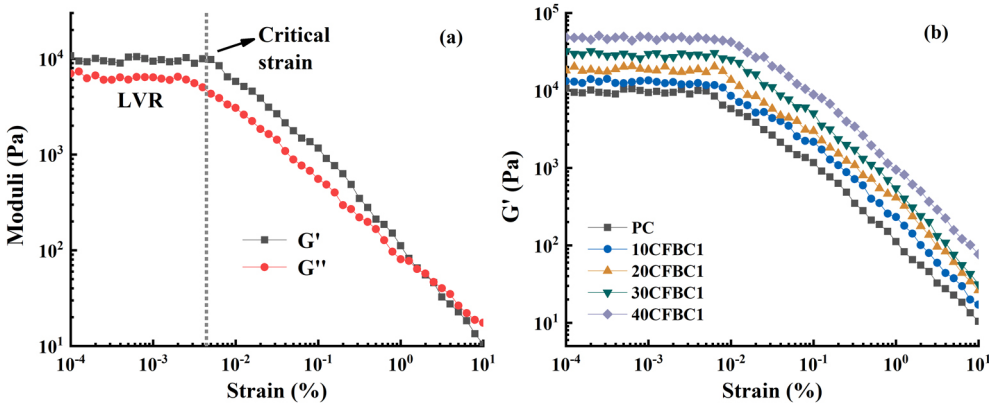

Fig. 9. Amplitude sweep curves of composite pastes showing: (a) Critical strain of PC-CFBCA mixes, (b) storage moduli

3.3.2. Time sweep

Figure 10 shows the time sweep results of the sample containing CFBC1, where Fig. 10(a)–(c) represent the development of G', G'', and δ over time, respectively. It can be observed that in these five samples, G' values are higher than G'', indicating that in the early stages of oscillation testing, PC-CFBC composites mostly exhibited elasticity. This can be proven from the result of phase angle δ, i.e., the phase angle of all pastes is within the range of 10–20°.

Both G' and G'' showed very rapid growth in the early stage of hydration, and then the growth rate began to slow down and remained stable. The paste containing 40% CFBC1 exhibits the highest G', demonstrating its most significant elasticity. It is worth noting that after the hydration time exceeds 60 min, the difference in G' and G'' values of pastes with different mix ratios begins to decrease, indicating that although pastes with low CFBC content have a relatively lower rate of early structural build-up, they grow faster in the later stage.

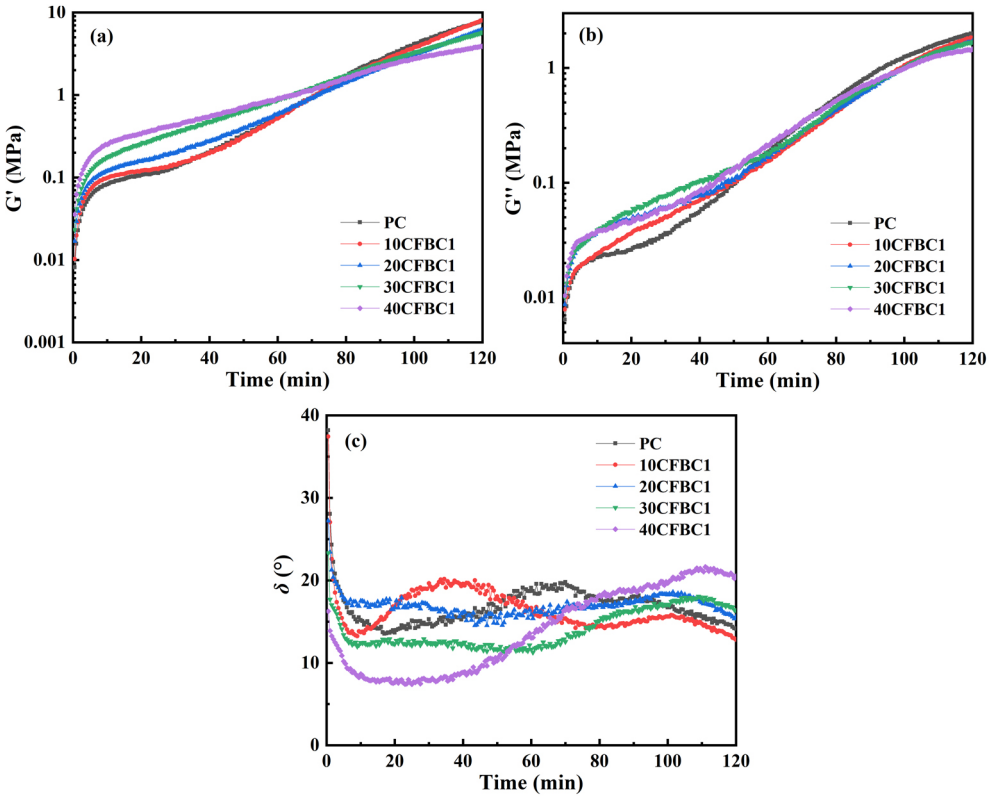

Fig. 10. Evolution of viscoelastic parameters of PC-CFBCA mixes with time showing: (a) Storage modulus, (b) loss modulus, (c) phase angle

3.4. Adsorption amount

In addition to the inherent properties of CFBC ash, its synergistic effect with PCE is also an important influencing factor on the rheological properties of composite pastes. After being added to the cement-water system, PCE will first adsorb with cement particles, and only then can they reduce water, disperse, and change the fluidity of the paste. According to surface chemistry, the adsorption modes of surfactants at solid-liquid interfaces mainly include ion adsorption, ion exchange adsorption, hydrogen bonding adsorption, and dispersion

force adsorption. When PCE is adsorbed on the surface of cement particles, it can act as a dispersant in four ways: (i) The adsorption of PCE causes the particle surface to carry the same charge, and the particles are kept dispersed through electrostatic repulsion; (ii) PCE separates cement particles through steric hindrance; (iii) PCE causes the disintegration of the coagulation structure in the cement paste and (iv) PCE delays the hydration rate of cement, thereby slowing down the rate of structural build-up of the paste [57, 58].

In order to further evaluate the changes in adsorption capacity of cement paste after the addition of CFBC ash, Fig. 11 shows the effect of different particle sizes of CFBC ash on the saturated adsorption amount. It can be seen that samples containing CFBC ash with smaller particle size exhibit higher adsorption capacity. This indicates that as the specific surface area of CFBC ash increases, the particle surface can provide more adsorption sites for PCE, thereby improving the overall adsorption efficiency of the system.

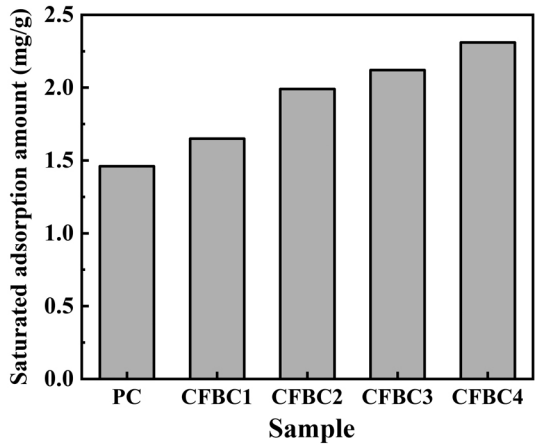

Fig. 11. Saturated adsorption amount of PCE in PC and CFBCA particles

3.5. Hydration process

The hydration process of cement significantly influences the initial rheological characteristics of the paste. A distinguishing feature of cement, unlike other inert suspension dispersion systems, is its reactive nature upon full mixing with water, ensuring continuous hydration. This ongoing hydration constitutes a pivotal factor driving the transition of the paste from initial plasticity to subsequent elasticity. To assess the hydration reaction rates across various samples, Fig. 12 illustrates the temporal evolution of heat flow and cumulative heat release for 13 sample groups. Generally, all hydration curves exhibit consistent features: intense heat release during the early hydration stages, characterized by elevated heat flow values, followed by an induction phase marked by stable, lower-level heat flow. Subsequent to this phase, hydration rates experience a resurgence, peaking at approximately 12 h. Quantitative analysis in Table 3 reveals that the addition of CFBC ash, particularly with larger particle sizes, marginally augments the reaction rate of composite pastes. However, the impact remains

limited, suggesting a modest influence of CFBC ash on the hydration dynamics of the PC system. Further exploration of this relationship between rheology and hydration characteristics is expounded upon in the following discussion section.

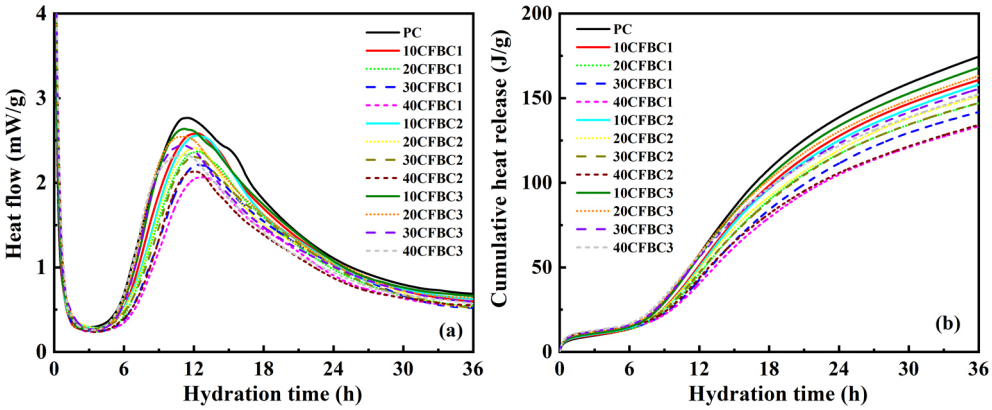

Fig. 12. Hydration heat release curve of composite pastes showing: (a) Heat flow, (b) cumulative heat release

Table 3. Kinetics parameters of hydration process of PC-CFBC fly ash paste

Sample	n	K_{NG}	K_I	K_D	α_1	α_2
PC	2.0122	0.052	0.0141	0.0027	0.1711	0.2612
10CFBC1	2.2167	0.0532	0.0151	0.0027	0.1783	0.2456
20CFBC1	2.3565	0.053	0.015	0.0027	0.1734	0.2423
30CFBC1	2.6164	0.0511	0.0146	0.0025	0.1662	0.2391
40CFBC1	2.748	0.0503	0.0145	0.0025	0.1636	0.2352
10CFBC2	2.4056	0.0526	0.0153	0.0027	0.1793	0.2406
20CFBC2	2.3505	0.052	0.0149	0.0025	0.1772	0.2348
30CFBC2	2.4458	0.0512	0.0145	0.0025	0.1701	0.2403
40CFBC2	2.4663	0.0519	0.0146	0.0024	0.1664	0.2282
10CFBC3	2.0122	0.0527	0.0142	0.0026	0.1713	0.2508
20CFBC3	1.8946	0.0524	0.0139	0.0025	0.1652	0.2481
30CFBC3	1.9035	0.0523	0.0138	0.0024	0.1635	0.2413
40CFBC3	1.8065	0.051	0.0134	0.0024	0.1626	0.2422

4. Discussion

4.1. Effect of PCE on thixotropy of PC-CFBC fly ash paste

Initially, the adsorption of PCE appears to exert the most pronounced influence on the thixotropy of the paste. This is attributed to PCE's role in diminishing the volume fraction of the flocculation structure within the system, a critical determinant of paste thixotropy. Upon the application of vigorous shear forces to the paste, its microstructure undergoes disruption, leading to the disintegration of the flocculation structure. Consequently, systems featuring a larger initial volume fraction of the flocculation structure exhibit greater viscosity disparities before and after shear application, indicative of heightened thixotropy. Against this backdrop, Fig. 13 illustrates the association between thixotropy and saturated adsorption quantity. Herein, the thixotropy of PC paste serves as the baseline, with the thixotropy and adsorption capacity ratios of other mixes relative to PC serving as the nominal values. Notably, the thixotropy of PC-CFBC ash composites demonstrates a positive correlation with adsorption quantity, implying that higher thixotropy corresponds to greater PCE adsorption. Additionally, CFBC3, characterized by a finer particle size distribution, yields enhanced paste thixotropy at equivalent adsorption capacities.

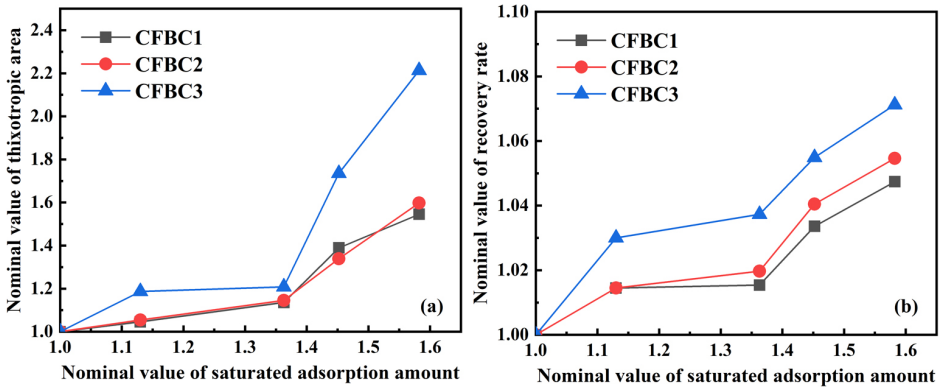

Fig. 13. Relationship between saturated adsorption amount and thixotropy of composite pastes

4.2. Viscoelasticity and hydration kinetics

As delineated in the preceding results, the process of cement hydration bears a close nexus with the viscoelastic properties of the paste, given that hydration stands as the primary impetus for the structural build-up of cement paste. Illustrated in Fig. 14 is the correlation between G', G'', and δ, with KNG. As anticipated, both G' and G'' exhibit a positive correlation with the hydration rate parameter KNG, signifying that an elevation in the hydration rate concurrently expedites the pace of viscoelastic evolution within the system. Conversely, the trend observed in δ runs counter to that of KNG. A diminution in the δ value signifies a predominance of the elastic component within the paste, indicative of a heightened rate of elastic development, thereby corroborating the findings derived from the viscoelasticity tests.

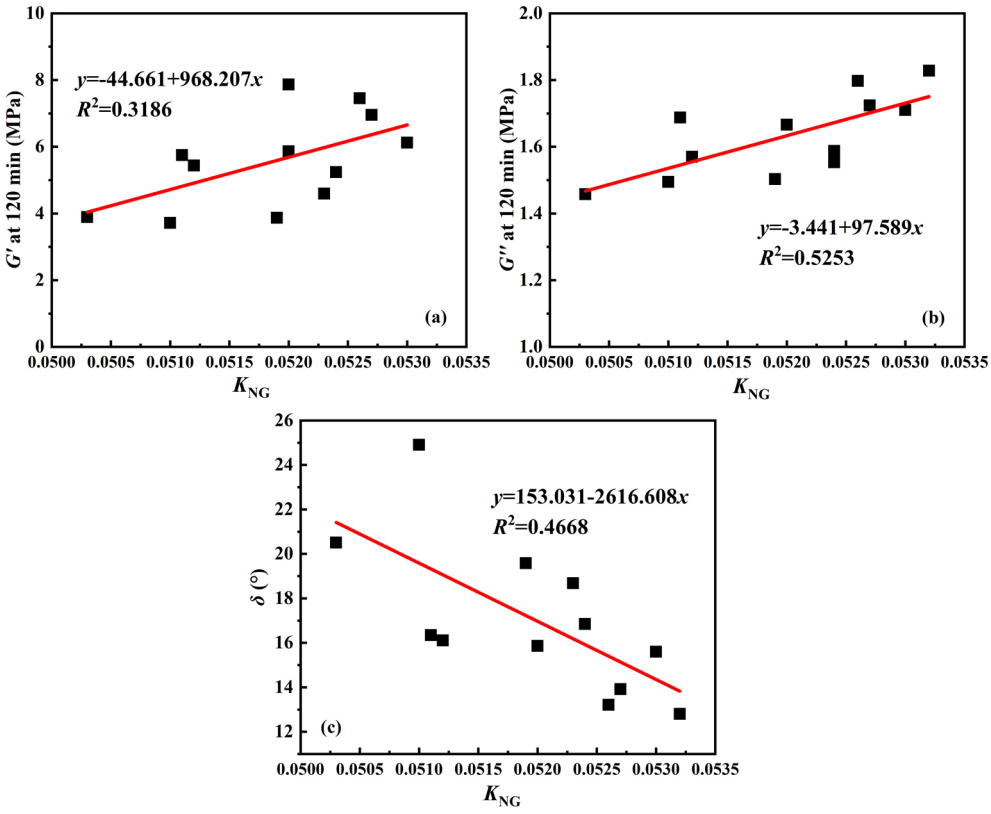

Fig. 14. Relationship between hydration kinetics parameter and viscoelastic parameters

5. Conclusions

This study mainly investigated the performance evolution of PC-CFBC ash composites from three aspects: rheology, cement hydration, and adsorption of PCE, and analyzed the influence mechanism of different types of CFBC ash on the rheological properties of the paste. The main conclusions that can be obtained are as follows:

1. The modified Bingham, Herschel–Bulkley, and Casson models effectively capture the rheological behaviors of PC-CFBC ash composites. Elevated CFBC content correlates with heightened yield stress and viscosity in the paste. Furthermore, incorporation of CFBC with finer particle size distribution amplifies these rheological parameters.
2. Thixotropic characteristics, encompassing hysteresis loop area and recovery rate, parallel shifts observed in dynamic yield stress and viscosity, showcasing improved thixotropy upon CFBC ash inclusion.
3. Within the five groups examined, G' predominates over G'', indicating predominantly elastic behavior during early oscillation testing. Subsequently, the discrepancy in G' diminishes as hydration progresses beyond 60 min across various mix proportions.

4. The thixotropy of PC-CFBC ash composites closely correlates with PCE adsorption capacity, while the hydration rate dictates the viscoelastic evolution of the paste. Enhanced hydration rates accelerate viscoelastic development, particularly reflected in G', thereby furnishing pivotal insights for optimizing the rheological properties of the composite system.

This study offers a thorough examination of the impact of CFBC ash on PC, considering three key aspects: rheological properties, hydration characteristics, and superplasticizer adsorption capacity. The findings derived from this analysis serve as a crucial foundation for enhancing the operational efficacy of the PC-CFBC ash system, thereby facilitating its enhanced utilization in scenarios demanding high workability standards, such as formwork pressure prediction and self-compacting concrete applications.

References

[1] W.T. Lin, K.L. Lin, K. Chen, K. Korniejenko, M. Hebda, and M. Łach, "Circulation fluidized bed combustion fly ash as partial replacement of fine aggregates in roller compacted concrete", *Materials*, vol. 12, no. 24, art. no. 4204, 2019, doi: 10.3390/ma12244204.

[2] Y. Peng and C. Unluer, "Modeling the mechanical properties of recycled aggregate concrete using hybrid machine learning algorithms", *Resources, Conservation and Recycling*, vol. 190, art. no. 106812, 2023, doi: 10.1016/j.resconrec.2022.106812.

[3] J. Shi, Y. Liu, H. Xu, Y. Peng, Q. Yuan, and J. Gao, "The roles of cenosphere in ultra-lightweight foamed geopolymer concrete (UFGC)", *Ceramics International*, vol. 48, no. 9, pp. 12884–12896, 2022, doi: 10.1016/j.ceramint.2022.01.161.

[4] Y. Nie, J. Shi, Z. He, B. Zhang, Y. Peng, and J. Lu, "Evaluation of high-volume fly ash (HVFA) concrete modified by metakaolin: Technical, economic and environmental analysis", *Powder Technology*, vol. 397, art. no. 117121, 2022, doi: 10.1016/j.powtec.2022.117121.

[5] J. Havlica, J. Brandstetr, and I. Odler, "Possibilities of utilizing solid residues from pressured fluidized bed coal combustion (PSBC) for the production of blended cements", *Cement and Concrete Research*, vol. 28, no. 2, pp. 299–307, 1998, doi: 10.1016/S0008-8846(97)00258-5.

[6] Y.H. Kang and Y.C. Choi, "Development of non-sintered zero-OPC binders using circulating fluidized bed combustion ash", *Construction and Building Materials*, vol. 178, pp. 562–573, 2018, doi: 10.1016/j.conbuildmat.2018.05.184.

[7] H.K. Lee, S.M. Jeon, B.Y. Lee, and H.K. Kim, "Use of circulating fluidized bed combustion bottom ash as a secondary activator in high-volume slag cement", *Construction and Building Materials*, vol. 234, art. no. 117240, 2020, doi: 10.1016/j.conbuildmat.2019.117240.

[8] X. Xun, F. Xiaoling, and Y. Chenglin, "Investigation on physical properties, strength and phase evolution of binary cementitious materials made of CFBC ash and lime", *Construction and Building Materials*, vol. 265, art. no. 120302, 2020, doi: 10.1016/j.conbuildmat.2020.120302.

[9] J. Lee, T. Lee, S. Lee, and H. Choi, "Performance Evaluation of Cementless Composites with Alkali-Sulfate Activator for Field Application", *Materials*, vol. 13, no. 23, art. no. 5410, 2020, doi: 10.3390/ma13235410.

[10] K. Chen, W.T. Lin, and W. Liu, "Microstructures and mechanical properties of sodium-silicate-activated slag/co-fired fly ash cementless composites", *Journal of Cleaner Production*, vol. 277, art. no. 124025, 2020, doi: 10.1016/j.jclepro.2020.124025.

[11] M. Niu, C. Liu, X. Wang, Y. Huang, L. Dong, L. Duan, L. Xu, Y. Wang, C. Sun, and H. Liu, "Chemical Characteristics of Ash Formed from the Combustion of Shoe Manufacturing Waste in a 2.5 MWth Circulating Fluidized Bed Combustor", *Waste and Biomass Valorization*, vol. 11, pp. 4551–4560, 2020, doi: 10.1007/s12649-019-00733-7.

[12] D. Carro-López, B. González-Fonteboa, J. Eiras-López, and S. Seara-Paz, "Comparing circulating fluidised bed fly ash and limestone as additions for cement", *Magazine of Concrete Research*, vol. 71, no. 24, pp. 1302–1311, 2019, doi: 10.1680/jmacr.18.00490.

[13] G. Sheng, Q. Li, and J. Zhai, "Investigation on the hydration of CFBC fly ash", *Fuel*, vol. 98, pp. 61–66, 2012, doi: 10.1016/j.fuel.2012.02.008.

[14] K. Ohenoja, J. Pesonen, J. Yliniemi, and M. Illikainen, "Utilization of fly ashes from fluidized bed combustion: A review", *Sustainability*, vol. 12, no. 7, art. no. 2988, 2020, doi: 10.3390/su12072988.

[15] S. Siddique and J.G. Jang, "Effect of CFBC ash as partial replacement of PCC ash in alkali-activated material", *Construction and Building Materials*, vol. 244, art. no. 118383, 2020, doi: 10.1016/j.conbuildmat.2020.118383.

[16] R. Wu, S. Dai, S. Jian, J. Huang, Y. Lv, B. Li, and N. Azizbek, "Utilization of the circulating fluidized bed combustion ash in autoclaved aerated concrete: Effect of superplasticizer", *Construction and Building Materials*, vol. 237, art. no. 117644, 2020, doi: 10.1016/j.conbuildmat.2019.117644.

[17] C. Wang, L. Jia, Y. Tan, and E.J. Anthony, "Carbonation of fly ash in oxy-fuel CFB combustion", in *Challenges of Power Engineering and Environment: Proceedings of the International Conference on Power Engineering 2007*. Berlin Heidelberg: Springer, 2007, pp. 799–804.

[18] H.S. Djayaprabha, T.P. Chang, J.Y. Shih, and H.A. Nguyen, "Improving the mechanical and durability performance of No-cement self-compacting concrete by fly ash", *Journal of Materials in Civil Engineering*, vol. 32, no. 9, art. no. 04020245, 2020, doi: 10.1061/(ASCE)MT.1943-5533.0003281.

[19] X. Fu, Q. Li, J. Zhai, G. Sheng, and F. Li, "The physical–chemical characterization of mechanically-treated CFBC fly ash", *Cement and Concrete Composites*, vol. 30, no. 3, pp. 220–226, 2008, doi: 10.1016/j.cemconcomp.2007.08.006.

[20] T. Wu, M. Chi, and R. Huang, "Characteristics of CFBC fly ash and properties of cement-based composites with CFBC fly ash and coal-fired fly ash", *Construction and Building Materials*, vol. 66, pp. 172–180, 2014, doi: 10.1016/j.conbuildmat.2014.05.057.

[21] G. Sheng, Q. Li, J. Zhai, and F. Li, "Self-cementitious properties of fly ashes from CFBC boilers co-firing coal and high-sulphur petroleum coke", *Cement and Concrete Research*, vol. 37, no. 6, pp. 871–876, 2007, doi: 10.1016/j.cemconres.2007.03.013.

[22] Y. Shen, J. Qian, and Z. Zhang, "Investigations of anhydrite in CFBC fly ash as cement retarders", *Construction and Building Materials*, vol. 40, pp. 672–678, 2013, doi: 10.1016/j.conbuildmat.2012.11.056.

[23] X. Xun, H. Zongyue, D. Liling, Z. Yudong, X. Yulong, and L. Weichao, "Investigation of high volume of CFBC ash on performance of basic magnesium sulfate cement", *Journal of Environmental Management*, vol. 256, art. no. 109878, 2020, doi: 10.1016/j.jenvman.2019.109878.

[24] H. Xu, Q. Li, L. Shen, W. Wang, and J. Zhai, "Synthesis of thermostable geopolymer from circulating fluidized bed combustion (CFBC) bottom ashes", *Journal of Hazardous Materials*, vol. 175, no. 1-3, pp. 198–204, 2010, doi: 10.1016/j.jhazmat.2009.09.149.

[25] Y. Xia, Y. Yan, and Z. Hu, "Utilization of circulating fluidized bed fly ash in preparing non-autoclaved aerated concrete production", *Construction and Building Materials*, vol. 47, pp. 1461–1467, 2013, doi: 10.1016/j.conbuildmat.2013.06.033.

[26] Z. Zhang, J. Qian, C. You, and C. Hu, "Use of circulating fluidized bed combustion fly ash and slag in autoclaved brick", *Construction and Building Materials*, vol. 35, pp. 109–116, 2012, doi: 10.1016/j.conbuildmat.2012.03.006.

[27] B.Y. Lee, S.M. Jeon, C.G. Cho, and H.K. Kim, "Evaluation of time to shrinkage-induced crack initiation in OPC and slag cement matrices incorporating circulating fluidized bed combustion bottom ash", *Construction and Building Materials*, vol. 257, art. no. 119507, 2020, doi: 10.1016/j.conbuildmat.2020.119507.

[28] N.T. Dung, T.P. Chang, C.T. Chen, and T.R. Yang, "Cementitious properties and microstructure of an innovative slag eco-binder", *Materials and Structures*, vol. 49, pp. 2009–2024, 2016, doi: 10.1617/s11527-015-0630-6.

[29] A. Machowska, Z. Kledyński, I. Wilińska, and B. Pacewska, "A study of the early hydration processes and properties of fly ash-slag binders", *Bulletin of Materials Science*, vol. 42, pp. 1–10, 2019, doi: 10.1007/s12034-019-1886-1.

[30] N.T. Dung, T.P. Chang, and C.T. Chen, "Circulating fluidized bed combustion fly ash-activated slag concrete as novel construction material", *ACI Materials Journal*, vol. 112, pp. 105–114, 2015, doi: 10.14359/51686910.

[31] N.T. Dung, T.P. Chang, and C.T. Chen, "Engineering and sulfate resistance properties of slag-CFBC fly ash paste and mortar", *Construction and Building Materials*, vol. 63, pp. 40–48, 2014, doi: 10.1016/j.conbuildmat.2014.04.009.

[32] H.J. Kim, M. Tafesse, H.K. Lee, and H.K. Kim, "Incorporation of CFBC ash in sodium silicate-activated slag system: Modification of microstructures and its effect on shrinkage", *Cement and Concrete Research*, vol. 123, art. no. 105771, 2019, doi: 10.1016/j.cemconres.2019.05.016.

[33] H.A. Nguyen, T.P. Chang, and J.Y. Shih, "Effects of sulfate rich solid waste activator on engineering properties and durability of modified high volume fly ash cement based SCC", *Journal of Building Engineering*, vol. 20, pp. 123–129, 2018, doi: 10.1016/j.jobe.2018.07.010.

[34] Z. Cheng, L. He, L. Liu, Z. Cheng, X. Pei, and Z. Ma, "Mechanical Properties and Durability of High-Performance Concretes Blended with Circulating Fluidized Bed Combustion Ash and Slag as Replacement for Ordinary Portland Cement", *Advances in Materials Science and Engineering*, vol. 2020, art. no. 8613106, 2020, doi: 10.1155/2020/8613106.

[35] S.M. Park, J.H. Seo, and H.K. Lee, "Binder chemistry of sodium carbonate-activated CFBC fly ash", *Materials and Structures*, vol. 51, pp. 1–10, 2018, doi: 10.1617/s11527-018-1183-2.

[36] J.G. Jang, S.M. Park, S. Chung, J.W. Ahn, and H.K. Kim, "Utilization of circulating fluidized bed combustion ash in producing controlled low-strength materials with cement or sodium carbonate as activator", *Construction and Building Materials*, vol. 159, pp. 642–651, 2018, doi: 10.1016/j.conbuildmat.2017.08.158.

[37] S.M. Park, N.K. Lee, and H.K. Lee, "Circulating fluidized bed combustion ash as controlled low-strength material (CLSM) by alkaline activation", *Construction and Building Materials*, vol. 156, pp. 728–738, 2017, doi: 10.1016/j.conbuildmat.2017.09.001.

[38] Y. Peng, K. Ma, G. Long, Y. Xie, L. Yu, and Q. Xie, "Effect of packing density according to CPM on the rheology of cement–fly ash–slag paste", *Journal of Materials in Civil Engineering*, vol. 33, no. 8, art. no. 04021209, 2021, doi: 10.1061/(ASCE)MT.1943-5533.0003823.

[39] S. Nazar, J. Yang, B.S. Thomas, I. Azim, and S.K.U. Rehman, "Rheological properties of cementitious composites with and without nano-materials: A comprehensive review", *Journal of Cleaner Production*, vol. 272, art. no. 122701, 2020, doi: 10.1016/j.jclepro.2020.122701.

[40] Y. Peng and C. Unluer, "Development of alternative cementitious binders for 3D printing applications: A critical review of progress, advantages and challenges", *Composites Part B: Engineering*, vol. 252, art. no. 110492, 2023, doi: 10.1016/j.compositesb.2022.110492.

[41] S. Paritala, K.K. Singaram, I. Bathina, M.A. Khan, and S.K.R. Jyosyula, "Rheology and pumpability of mix suitable for extrusion-based concrete 3D printing – A review", *Construction and Building Materials*, vol. 402, art. no. 132962, 2023, doi: 10.1016/j.conbuildmat.2023.132962.

[42] Y. Peng and C. Unluer, "Advances in rheological measurement and characterization of fresh cement pastes", *Powder Technology*, vol. 429, art. no. 118903, 2023, doi: 10.1016/j.powtec.2023.118903.

[43] L. Guan, X. Liu, and X. Liu, "Effect of hydroxypropyl methyl cellulose on rheological properties of cement-limestone paste", *Archives of Civil Engineering*, vol. 69, no. 1, pp. 593–612, 2023, doi: 10.24425/ace.2023.144190.

[44] J.T. Kolawole, R. Combrinck, and W.P. Boshoff, "Shear rheo-viscoelasticity approach to the plastic cracking of early-age concrete", *Cement and Concrete Research*, vol. 135, art. no. 106127, 2020, doi: 10.1016/j.cemconres.2020.106127.

[45] Y. Zhang, X. Kong, L. Gao, Z. Lu, S. Zhou, B. Dong, and F. Xing, "In-situ measurement of viscoelastic properties of fresh cement paste by a microrheology analyzer", *Cement and Concrete Research*, vol. 79, pp. 291–300, 2016, doi: 10.1016/j.cemconres.2015.09.020.

[46] Y. Peng and C. Unluer, "Investigation of the viscoelastic evolution of reactive magnesia cement pastes with accelerated hydration mechanisms", *Cement and Concrete Composites*, vol. 142, art. no. 105191, 2023, doi: 10.1016/j.cemconcomp.2023.105191.

[47] J.T. Kolawole, R. Combrinck, and W.P. Boshoff, "Rheo-viscoelastic behaviour of fresh cement-based materials: Cement paste, mortar and concrete", *Construction and Building Materials*, vol. 248, art. no. 118667, 2020, doi: 10.1016/j.conbuildmat.2020.118667.

[48] Y. Qian, K. Lesage, K. El Cheikh, and G. De Schutter, "Effect of polycarboxylate ether superplasticizer (PCE) on dynamic yield stress, thixotropy and flocculation state of fresh cement pastes in consideration of the Critical Micelle Concentration (CMC)", *Cement and Concrete Research*, vol. 107, pp. 75–84, 2018, doi: 10.1016/j.cemconres.2018.02.019.

[49] Y. Peng, K. Ma, G. Long, and Y. Xie, "Influence of nano-SiO_2, nano-$CaCO_3$ and nano-Al_2O_3 on rheological properties of cement–fly ash paste", *Materials*, vol. 12, no. 16, art. no. 2598, 2019, doi: 10.3390/ma12162598.

[50] T. Huang, Q. Yuan, F. He, and Y. Xie, "Understanding the mechanisms behind the time-dependent viscoelasticity of fresh C3A–gypsum paste", *Cement and Concrete Research*, vol. 133, art. no. 106084, 2020, doi: 10.1016/j.cemconres.2020.106084.

[51] Z. Xue, D. Gan, Y. Zhang, and Z. Liu, "Rheological behavior of ultrafine-tailings cemented paste backfill in high-temperature mining conditions", *Construction and Building Materials*, vol. 253, art. no. 119212, 2020, doi: 10.1016/j.conbuildmat.2020.119212.

[52] M. Chen, L. Yang, Y. Zheng, Y. Huang, L. Li, P. Zhao, S. Wang, L. Lu, and X. Cheng, "Yield stress and thixotropy control of 3D-printed calcium sulfoaluminate cement composites with metakaolin related to structural build-up", *Construction and Building Materials*, vol. 252, art. no. 119090, 2020, doi: 10.1016/j.conbuildmat.2020.119090.

[53] Y. Qian and G. De Schutter, "Enhancing thixotropy of fresh cement pastes with nanoclay in presence of polycarboxylate ether superplasticizer (PCE)", *Cement and Concrete Research*, vol. 111, pp. 15–22, 2018, doi: 10.1016/j.cemconres.2018.06.013.

[54] L. Liu, P. Yang, C. Qi, B. Zhang, L. Guo, and K.I. Song, "An experimental study on the early-age hydration kinetics of cemented paste backfill", *Construction and Building Materials*, vol. 212, pp. 283–294, 2019, doi: 10.1016/j.conbuildmat.2019.03.322.

[55] L. Zhou, M. Gou, and X. Guan, "Hydration kinetics of cement-calcined activated bauxite tailings composite binder", *Construction and Building Materials*, vol. 301, art. no. 124296, 2021, doi: 10.1016/j.conbuildmat.2021.124296.

[56] B. Zhaidarbek, A. Tleubek, G. Berdibek, and Y. Wang, "Analytical predictions of concrete pumping: Extending the Khatib–Khayat model to Herschel–Bulkley and modified Bingham fluids", *Cement and Concrete Research*, vol. 163, art. no. 107035, 2023, doi: 10.1016/j.cemconres.2022.107035.

[57] Y. Zhang and X. Kong, "Correlations of the dispersing capability of NSF and PCE types of superplasticizer and their impacts on cement hydration with the adsorption in fresh cement pastes", *Cement and Concrete Research*, vol. 69, pp. 1–9, 2015, doi: 10.1016/j.cemconres.2014.11.009.

[58] J. Plank, B. Sachsenhauser, and J. De Reese, "Experimental determination of the thermodynamic parameters affecting the adsorption behaviour and dispersion effectiveness of PCE superplasticizers", *Cement and Concrete Research*, vol. 40, no. 5, pp. 699–709, 2010, doi: 10.1016/j.cemconres.2009.12.002.

Received: 2024-02-29, Revised: 2024-04-04